Defense Technical Information Center
Compilation Part Notice

ADP013661

TITLE: Large-Eddy Simulation of Square Jet

DISTRIBUTION: Approved for public release, distribution unlimited

This paper is part of the following report:

TITLE: DNS/LES Progress and Challenges. Proceedings of the Third
AFOSR International Conference on DNS/LES

To order the complete compilation report, use: ADA412801

The component part is provided here to allow users access to individually authored sections
of proceedings, annals, symposia, etc. However, the component should be considered within
the context of the overall compilation report and not as a stand-alone technical report.

The following component part numbers comprise the compilation report:
ADP013620 thru ADP013707

LARGE-EDDY SIMULATION OF SQUARE JET

X. ZHOU AND D. D. KNIGHT
Department of Mechanical and Aerospace Engineering
Rutgers University
98 Brett Road
Piscataway, NJ 08854-8058
USA

Abstract. We present a large-eddy simulation (LES) of the near-field of a low-Mach number square jet. The filtered governing equations of compressible flows are solved using the approximate Riemann solver of Roe for the convective fluxes and an application of Gauss' theorem for the viscous fluxes on an unstructured grid of tetrahedral cells. The LES is performed with the Monotone Integrated LES (MILES) for the subgrid scale model. A square jet at a Mach number of 0.3 and a Reynolds number of 3,200 is simulated. Axis-rotation occurs and is caused by Biot-Savart self-induction associated with nonuniform shear-layer curvature at the exit. Complex vortex topologies and interaction between vortex rings and rib vortices are observed downstream. Mean properties are in good agreement with the Direct Numerical Simulation (DNS) results of Grinstein et al. (1995).

1. Introductions

Turbulent round and plane jets are simple inhomogeneous flows that can be served to verify models for complex flows and have been experimentally and numerically studied extensively [1, 2]. Recently, noncircular jets have been gained much interest in passive control due to their enhanced jet mixing properties [3, 4, 5, 6, 7].

In the past, Reynolds-Averaged Numerical Simulations (RANS) have often been employed for the investigation of jet flows. However, this kind of traditional method cannot give a clear picture of the unsteady behaviour and the results are too sensitive to the turbulence models used. The advantage of Direct Numerical Simulation (DNS) [8] and Large Eddy Simulation

(LES) [9] in being able to capture a wide range of spatial scales and temporal scales is of great value for fundamental and applied studies. LES is a good alternative to DNS which is more expensive for high Reynolds number flows. One of the practical uses of LES is to predict the transition and subsequent turbulent mixing (or spreading) process that occurs in spatially developing flows.

As is well known, a free jet is subject to Kelvin-Helmholtz instability which, in turn, means that the flow experiences an exponentially growing instability and results in rolling up of vortices, pairing and merging processes. Linear instability analyses have confirmed this growth. The subsequent breakdown of the large-scale vortical structures is followed by the advent of spreading by the secondary three-dimensional instability mechanism. Vortex dynamics are also expected to be important in the control of noncircular jets instability, transition from laminar to turbulence and the jet development further downstream. Grinstein and DeVore [3] showed a transition to turbulence in free square jets characterized by the dynamics of vortex rings and braid vortices and observed a larger entrainment rate compared to round jets. The underlying mechanism for the enhanced entrainment is the self-induced axis-rotation or axis-switching resulting from Biot-Savart deformation of vortex rings caused by non-uniform azimuthal curvature at the jet exit. Foss and Zaman [10] and Zaman [11] analyzed the influence of jet geometry on the characteristics of spreading in subsonic and supersonic flows. They observed a substantial increase of jet spreading when tabs were inserted at the nozzle which induced streamwise vortex pairs.

The objective of this research is to validate the present MILES methodology using an unstructured grid for a subsonic square jet. First, the implementation techniques of solving the governing equations are discussed briefly using an approximate Riemann solver of Roe's method and the SGS model for the unresolved small scales in the LES. Secondly, a square jet at a Reynolds number of 3,200 and a Mach number of 0.3 is simulated. Temporal evolutions are visualized to characterize the dynamics of deforming vortex rings, ribs and their interactions. Statistical quantities are quantified and compared with the DNS results of Grinstein et al [3].

2. Governing equations

The present LES method is based on solving the 3-D time-dependent nondimensional filtered transport equations for mass, momentum and energy and the state equation of ideal gas for fully compressible flows in an unstructured grid of tetrahedral cells using a cell-centered finite volume formation. Following are the nondimensionalized governing equations and the reference

quantities are: velocity U_∞, static temperature T_∞, density ρ_∞, length scale L and viscosity μ_∞, resulting in a Mach number of $M_\infty = U_\infty/\sqrt{\gamma R T_\infty}$ and a Reynolds number of $Re = \rho_\infty U_\infty L/\mu_\infty$.

$$\frac{\partial \overline{\rho}}{\partial t} + \frac{\partial}{\partial x_j}(\overline{\rho}\tilde{u}_j) = 0 \tag{1}$$

$$\frac{\partial(\overline{\rho}\tilde{u}_i)}{\partial t} + \frac{\partial(\overline{\rho}\tilde{u}_i\tilde{u}_j)}{\partial x_j} = -\frac{\partial \overline{p}}{\partial x_i} + \frac{\partial \tau_{ij}}{\partial x_j} + \frac{\partial \overline{\sigma}_{ij}}{\partial x_j} \quad (i = 1, 2, 3) \tag{2}$$

$$\frac{\partial(\overline{\rho}\tilde{e})}{\partial t} + \frac{\partial(\overline{\rho}\tilde{e} + \overline{p})\tilde{u}_j}{\partial x_j} = \frac{\partial}{\partial x_j}\left(Q_j + \overline{q}_j + (\tau_{ij} + \overline{\sigma}_{ij})\tilde{u}_i\right) \tag{3}$$

$$\overline{p} = \frac{\overline{\rho}\tilde{T}}{\gamma M_\infty^2} \tag{4}$$

where summation over the three coordinate directions is implied in terms with repeated indices, $\tilde{u}_i = \overline{\rho u_i}/\overline{\rho}$, and $\tilde{e} = \overline{\rho e}/\overline{\rho}$ are the Favre-filtered velocity and total energy, $\overline{p}$ is the pressure, $\overline{\rho}\tilde{e} = \overline{p}/(\gamma-1) + \frac{1}{2}\tilde{u}_k\tilde{u}_k$ is the total energy. $q_j = \frac{\mu}{RePr(\gamma-1)M^2}\frac{\partial \tilde{T}}{\partial x_j}$ is the molecular heat flux, where $Pr = 0.72$ is the molecular Prandtl number. The dimensionless molecular viscosity is dependent on temperature, $\mu = T^n$, where $n = 0.76$. The subgrid scale (SGS) stress is $\tau_{ij} = \overline{\rho u_i u_j} - \overline{\rho}\tilde{u}_i\tilde{u}_j$, the SGS heat transfer is $Q_j = \overline{\rho}(\widetilde{u_j T} - \tilde{u}_j\tilde{T})$, and the molecular viscous stress is $\overline{\sigma}_{ij} = \frac{\mu}{Re}[-\frac{2}{3}\frac{\partial \tilde{u}_k}{\partial x_k}\delta_{ij} + (\frac{\partial \tilde{u}_i}{\partial x_j} + \frac{\partial \tilde{u}_j}{\partial x_i})]$. The SGS terms τ_{ij} and Q_j are modeled by the MILES method ($\tau_{ij} = 0$ and $Q_j = 0$) to account for the unresolved small scale turbulence [12]. Although many advanced SGS models have been developed, the simple models such as the MILES are widely used.

The inviscid fluxes are computed by an approximate Riemann solver of Roe's flux difference splitting method [13], and Gauss' theorem is applied for the viscous fluxes and heat transfer. A second-order Runge-Kutta scheme is used for the time marching, and the time step is determined such that the total CFL (Courant-Friedrichs-Lewy) number is less than 1.0. The gradients of each variable $(\overline{\rho}, \overline{\rho}\tilde{u}, \overline{\rho}\tilde{v}, \overline{\rho}\tilde{w}, \overline{\rho}\tilde{e})$ in a cell are computed using Least Squares (LS) method of Singular Value Decomposition (SVD), where eight neighboring stencil cells are used. More details of the numerical procedure can be found in Ref. [14, 15].

The present MILES method has been validated for several benchmark problems. In Okong'o, Knight and Zhou [14], good agreement was achieved for the energy spectrum in an isotropic turbulent flow; also, the comparisons with the DNS and experiment were good for a channel flow. A LES of a supersonic flat plate boundary layer was successfully validated by comparing with experimental and theoretical results [16].

3. Details of Computation

A free square jet of width D at Reynolds number of 3,200 and Mach number of 0.3 is studied. The grid consists of $65 \times 65 \times 65$ hexahedral cells in an unstructured grid covering a computational domain of $5D$ in the streamwise direction and $\pm 3D$ along the transverse directions. Each hexahedral cell is divided into five tetrahedral cells, yielding a total of 1.3M tetrahedra. A uniform grid is used along the streamwise direction with the hexahedral grid spacing of $\Delta x/D = 0.078$, which is larger than 0.04 used by Grinstein et al. in their DNS [3]. The grids are stretched along the other two directions and the minimum grid spacings are $\Delta y/D = \Delta z/D = 0.0375$. The imposed boundary conditions include inflow, outflow and wall boundaries. At the inflow, the streamwise velocities are prescribed as

$$u = U[1 + A\sin(2\pi ft)] \qquad (5)$$

and

$$U = 0.5\,U_\infty\,[1 - \tanh[b_2(2|y|/D - D/(2|y|))] \times$$
$$0.5\,U_\infty\,[1 - \tanh[b_2(2|z|/D - D/(2|z|))], \qquad (6)$$

where $A = 0.02$ is the perturbation amplitude, f is the forcing frequency ($f = 0.5$), $b_2 = 0.25R_{\frac{1}{2}}/\theta$, where $R_{\frac{1}{2}}/\theta = 40$, $R = D/2$ and θ is the momentum thickness. Zero-gradient condition is imposed at the outlet and symmetry boundary conditions are used at the side walls.

4. LES Results

4.1. VORTEX DYNAMICS AND TOPOLOGY

The iso-surfaces of the total vorticity $\omega = \sqrt{\omega_x^2 + \omega_y^2 + \omega_z^2}$ corresponding to $\omega = 0.25\omega_{peak}$ are shown in Fig. 1. Azimuthal nonuniformities make the evolution of the jet shear layer more complicated relative to circular jets. Close to the jet exit, a smooth square vortex sheet can be observed, and subsequently rolled-up vortex-ring structures form due to shear-layer Kelvin-Helmholtz instability. However, the vortex rings further downstream deform to non-planar shape due to self-induction mechanism caused by azimuthal nonuniformities. The deformed vortex rings are connected with the four corners of the initial square sheet by ribs. The hairpin braid vortices aligned with the corners progress faster in the diagonal direction than the others, "which results in redistribution of energy between azimuthal and streamwise vortices" [5]. Further downstream, the jet development is characterized by the strong interaction between vortex rings and braid vortices, which leads to a final breakdown of the large-scales coherent structures

and transition to the turbulent flow. The self-induced deformation of the rings and rib pair were explained to be the leading mechanism for larger entrainment properties in non-circular jets relative to circular jets [7]. "The interactions between the streamwise vortices and the vortex rings is reminiscent of the interaction between ribs and spanwise rollers in the mixing layer" [7]. Mixing of jets with surroundings can be enhanced through controlling the formation, development and interaction of large-scale coherent structures passively.

Fig. 2 shows the instantaneous crosswise vorticity $\omega_z = \partial v/\partial x - \partial u/\partial y$ contours at a central $x-y$ plane. Rolled-up structures can be observed near the base, and subsequently symmetrical counterrotating toroidal structures form in the shear layer which are then followed by their stretching and deformation. The organized structures can be broken down into smaller eddies further downstream. Evidently, the MILES model can capture the transition process. Large-scale vortex rings dominate in the near-field and the small vortices dominate downstream after the breakdown. The spatial spreading can be clearly observed downstream as the jet spreads by entraining mass from the surrounding nonvortical fluid.

Fig. 3 (a-d) shows the contours of instantaneous streamwise vorticity, $\omega_x = \partial v/\partial z - \partial w/\partial y$, across the $y-z$ planes of $x/D = 1, 2, 3$ and 4. Quite different behaviour can be observed at different axial positions. Vortex shears with some rounded-corners are stretched and thickened but still keep the initial square shape at the position of $x/D = 1$. The jet cross section switches axis 45° relative to that of the jet nozzle at the axial location of $x/D = 2, 3$ due to self-induced velocity around the corners by the presence of streamwise vorticity. The flow structure develops into a irregular shape further downstream at $x/D = 4$.

4.2. JET MIXING AND ENTRAINMENT

The statistical quantities are obtained by averaging over 5 forcing cycles after a statistically stationary state has been reached after an elapsed dimensionless physical time of 10.

The centerline distributions of the mean axial velocity by LES compared with the DNS results of Grinstein et al. [3] are plotted in Fig. 4. The mean velocity initially decays within the first 1.5 diameters and subsequently shows a slight increase due to the periodic roll-up by the sinusoidal forcing. The decay after 3.2 diameters is the result of turbulent mixing. In general, the agreement between present MILES and previous DNS results are good.

The corresponding centerline r.m.s. velocities u'/U_c are shown in Fig. 5. Note that close to the inflow plane the r.m.s. of velocity fluctuations is about 2 percent and corresponds to the imposed disturbance level. In the

potential core region, the r.m.s. velocity decreases slightly with increasing axial distance which shows a tendency to remain laminar with low turbulence intensities. Beyond the end of the potential core, the fluctuations of velocity increase very rapidly, which indicates the appearance of the secondary-instability mechanism which leads to the final breakdown of the large vortex structures. Due to insufficient length scale in the streamwise direction, the self-similar behaviour has not been achieved. However, it can be seen that the agreement between MILES and DNS is very good for the transient square jet.

5. Conclusions

A subsonic free square jet of Mach 0.3 and Reynolds number of 3,200 has been investigated by the MILES using an unstructured grid. Self-induced axis-switching occurs due to azimuthal non-uniformity at the exit. Complex vortex topologies and interaction between vortex rings and rib vortices are observed downstream. The mean properties are in good agreement with the DNS results of Grinstein et al. [3].

6. Acknowledgment

References

1. Panchapakesan, N. R. and Lumley, J. L., Turbulence Measurements in Axisymmetric Jets of Air and Helium. Part 1. Air Jet (1993) *J. Fluid Mech.*, **Vol. 246**, pp. 197-223
2. Rodi, W., Turbulence Models and Their Application in Hydraulics-A State of the Art Review (1980), IAHR, Delft
3. Grinstein, F. F., Gutmark, E. and Parr, T. Near Field Dynamics of Subsonic Free Square Jets. A Computational and Experimental Study (1995), *Physics of Fluids*, **Vol. 7 no. 6**, pp. 1483–1497
4. Grinstein, F. F. and Kailasanath, K. (1995) Three-dimensional Numerical Simulations of Unsteady Reactive Square Jets, *Combustion and Flame*, **Vol. 100**, pp. 2–10
5. Grinstein, F. F. Vortex Dynamics and Entrainment in Rectangular Free Jets (2001) *J. Fluid Mech.*, **Vol. 437**, pp. 69–101
6. Gutmark, E. J. and Grinstein, F. F., Flow Control with Noncircular Jets (1999) *Annu. Rev. Fluid Mech.*, **Vol. 31**, pp. 239–272
7. Grinstein, F. F. and DeVore C. R., Coherent Structure Dynamics in Spatially-Developing Square Jets (1992) *AIAA-92-3441*

8. Boersma, G. J., Brethouwer, G. and Nieuwstadt, F. T. M., A numerical investigation on the effect of the inflow conditions on the self-similar region of a round jet (1996) *Phys. Fluids*, **Vol. 8**, pp. 899–909

9. Le Ribault, C., Sarkar, S. and Stanley, S. A., Large eddy simulation of a plane jet (1999) *Phys. Fluids*, **Vol. 11**, pp. 3069–3083

10. Foss, J. K. and Zaman, K.B.M.Q., Large- and Small-scale Vortical Motions in a Shear Layer Perturbed by Tabs (1999) *J. Fluid Mech.*, **Vol. 382**, pp. 307–329

11. Zaman, K.B.M.Q., Spreading Characteristics of Compressible Jets From Nozzles of Various Geometries (1999) *J. Fluid Mech.*, **Vol. 383**, pp. 197–228

12. Fureby, C., On Subgrid Scale Modeling in Large Eddy Simulations of Compressible flow (1996) *Phys. Fluids*, **Vol. 5**, pp. 1301–1311

13. Hirsch, C., Numerical Computation of Internal and External Flows - Volume 2: Computational Methods for Inviscid and Viscous Flows, Wiley (1997), pp. 204–210

14. Okong'o, N., Knight, D. and Zhou, G., Large Eddy Simulations Using an Unstructured Grid Compressible Navier-Stokes Algorithm (2000) *Int. J. Computational Fluid Dynamics* , **Vol. 13 no. 13**, pp. 303-326

15. Urbin, G., Knight, D. and Zheltovodov, A., Compressible Large Eddy Simulation Using Unstructured Grid: Supersonic Turbulent Boundary Layer and Compression Corner (2000) *AIAA 2000-0427*

16. Urbin, G. and Knight, D., Large Eddy Simulation of a Supersonic Boundary Layer Using an Unstructured Grid (2001) *AIAA J.*, **Vol. 39 no. 7**, pp. 1288–1295
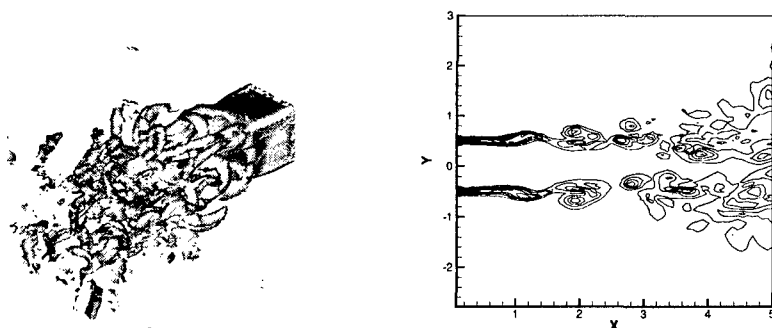
Figure 1. Instantaneous isosurfaces of total vorticity $\omega = 0.25\omega_{peak}$.

Figure 2. Instantaneous streamsise vorticity contours at the $x - y$ centre-plane.
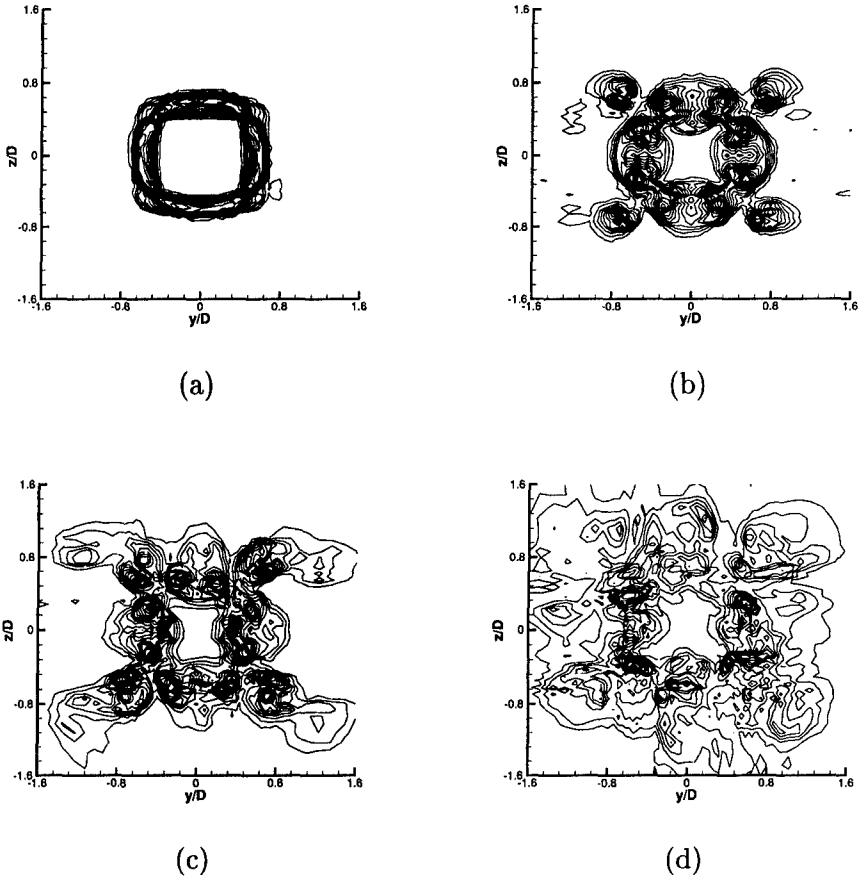
(a)

(b)

(c)

(d)

Figure 3.   Instantaneous streamwise vorticity contours across the $y - z$ planes at x/D = (a) 1, (b) 2, (c) 3 and (d) 4.
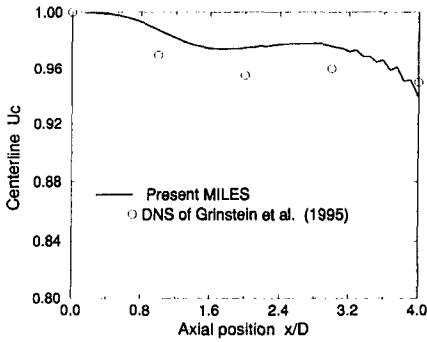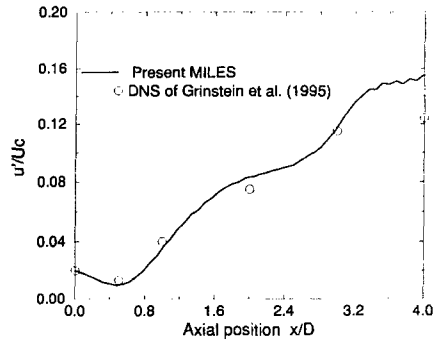

Figure 4.   Centerline profiles of the mean velocity.

Figure 5.   Centerline profiles of the r.m.s. axial velocity.